Thin-Film Photovoltaics

International Edition: DOI: 10.1002/anie.201603608
German Edition: DOI: 10.1002/ange.201603608

Pure Cubic-Phase Hybrid Iodobismuthates $AgBi_2I_7$ for Thin-Film Photovoltaics

*Younghoon Kim, Zhenyu Yang, Ankit Jain, Oleksandr Voznyy, Gi-Hwan Kim, Min Liu, Li Na Quan, F. Pelayo García de Arquer, Riccardo Comin, James Z. Fan, and Edward H. Sargent**

Abstract: *Bismuth-based hybrid perovskites are candidates for lead-free and air-stable photovoltaics, but poor surface morphologies and a high band-gap energy have previously limited these hybrid perovskites. A new materials processing strategy to produce enhanced bismuth-based thin-film photovoltaic absorbers by incorporation of monovalent silver cations into iodobismuthates is presented. Solution-processed $AgBi_2I_7$ thin films are prepared by spin-coating silver and bismuth precursors dissolved in n-butylamine and annealing under an N_2 atmosphere. X-ray diffraction analysis reveals the pure cubic structure (Fd3m) with lattice parameters of $a=b=c=$ 12.223 Å. The resultant $AgBi_2I_7$ thin films exhibit dense and pinhole-free surface morphologies with grains ranging in size from 200–800 nm and a low band gap of 1.87 eV suitable for photovoltaic applications. Initial studies produce solar power conversion efficiencies of 1.22 % and excellent stability over at least 10 days under ambient conditions.*

Solution-processed photovoltaic materials offering low cost and high-efficiency have been investigated for the photovoltaic conversion of solar into electrical power.[1–7] Organolead halide perovskites have advanced rapidly as promising solar absorbers with their power conversion efficiencies (PCE) now exceeding 22 % in thin-film photovoltaic devices.[7] This is a significant advance, since this PCE is on par with that of other thin-film solar cells, such as cadmium telluride (CdTe), copper–indium–gallium selenide (CIGS), and copper–zinc–tin sulfide (CZTS).[7]

While their progress in performance has been stunning, the reliance on lead in organolead perovskites could impact their commercial potential. This has increased interest in lead-free perovskites and analogues. Tin-based perovskites have been considered in this vein;[8,9] however, their device stability is impeded by the tin cation (Sn^{2+}), which is prone to disproportionation or oxidation when exposed to air and moisture, as well as raising toxicity concerns of their own.[10]

Bismuth, a trivalent cation, is a promising transition metal and non-toxic element to replace lead and tin.[10] Bismuth halides with the two-dimensional (2D) layered structures have been found to convert into perovskite-like hybrid structures when an appropriate organic cation such as 5,5‴-bis(aminoethyl)-2,2′:5′,2″:5″,2‴-quaterthiophene (AEQT),[11] diammonium ion[12] is included. This approach stabilizes the metal sites vacant through vacancy formation. Bismuth-based hybrid perovskites with complex crystal structures were recently investigated in the context of solar energy conversion.[13–15] Formed by the incorporation with methylammonium (MA^+) or cesium (Cs^+) cations into the octahedral bismuth iodide complex, crystalline $A_3B_2X_9$ (where A = MA or Cs, B = bismuth, X = Cl, Br, or I) films can be prepared by facile solution processing and used as photovoltaic absorbers in mesoscopic architectures.[13,15] Poor surface morphologies, including pinholes, combined with a relatively high band-gap energy ($E_g > 2.1$ eV), have so far limited bismuth-based perovskite devices to a solar PCE of 1.09 %, the best value reported to date for bismuth-based perovskite active materials.[13,15] Recently, a layer-structured bismuth triiodide (BiI_3) with lower E_g (ca. 1.8 eV) has also been considered as a promising candidate for thin-film solar cell photoactive materials.[16] However, to date, the best PCE of BiI_3-based devices is approximately three times lower than that of bismuth-based perovskites.

More recently, double-perovskite bulk crystals based on bismuth- and silver-halides (for example, $Cs_2AgBiBr_6$ and $Cs_2AgBiCl_6$) have been reported. Similarly to organolead halide perovskites, they exhibit a high tolerance to defects owing to the strongly ionic nature of the constituents.[17] The large E_g in these materials prevents absorption of much of the solar spectrum.[18,19]

We therefore pursued a new approach to solution-processed bismuth-based thin-film photovoltaic absorbers, one that would seek lead-free air-stable materials having a sufficiently low E_g to allow, in principle, wider spectral absorption.

Iodobismuthates based on the bismuth iodide complex have attracted considerable attention from organic/inorganic material chemists because of their potential electrical and optical properties, as well as their high solubility at room temperature.[20–24] The three-dimensional (3D) materials are more favorable than 2D materials in view of their semiconducting properties, and many studies have therefore focused on increasing the dimension of iodobismuthates by incorporating the organic and inorganic materials, leading to hybrid iodobismuthates.[20–24] To extend the dimension of the inorganic network and simultaneously control the band position of the active materials, the transition metal mono-

[*] Dr. Y. Kim, Dr. Z. Yang, Dr. A. Jain, Dr. O. Voznyy, Dr. G.-H. Kim, Dr. M. Liu, L. N. Quan, Dr. F. P. García de Arquer, Dr. R. Comin, J. Z. Fan, Prof. Dr. E. H. Sargent
Department of Electrical and Computer Engineering
University of Toronto
10 King's College Road, Toronto, Ontario, M5S 3G4 (Canada)
E-mail: ted.sargent@utoronto.ca

Supporting information for this article can be found under: http://dx.doi.org/10.1002/anie.201603608.

valent silver and copper cations (Ag^+ and Cu^+) have been introduced into these systems to connect the neighboring iodobismuthate units and achieve high dimensional (that is, 3D) materials.[20–22]

Until now, materials using Ag^+ and Cu^+ have been limited to structural and physical investigations (and no reports of solar performance) instead focusing on the use of complex anions, oligomeric clusters and polymeric infinite chains: indeed solution-processed solar cells based on silver iodobismuthates have never been reported. It is now known that silver-bismuth-iodine ternary systems (Ag-Bi-I), belonging to the silver iodobismuthate family, do crystallize to $AgBi_2I_7$ and Ag_2BiI_5; but again only the bulk crystals (and not films) have been synthesized, and structure-property relationships characterized therein.[25,26]

Herein, we present for the first solution-based synthesis of air-stable Ag-Bi-I thin-films. Specifically, we develop the fabrication of $AgBi_2I_7$ thin-films and deploy them towards solar energy harvesting. We used n-butylamine as the solvent to dissolve bismuth iodide (BiI_3) and silver iodide (AgI) and yield a homogeneous precursor solution. After spin-casting and annealing under inert atmosphere, the precursors cocrystallize and yield uniform $AgBi_2I_7$ thin-films (see Experimental Section in the Supporting Information). The resulting $AgBi_2I_7$ thin-films exhibit dense, smooth, and pinhole-free surface morphologies with large grains of 200–800 nm in size and an E_g value of 1.87 eV, that is, an absorption onset at 750 nm. The best PCE of our $AgBi_2I_7$ solar cell devices is 1.22 %. We also find that the $AgBi_2I_7$ devices show encouraging stability over 10 days under ambient conditions.

Unlike BiI_3, the AgI precursor is insoluble in polar aprotic solvents such as dimethylformamide (DMF) and dimethyl sulfoxide (DMSO), which are used as a solvent to solubilize the metal halides. Since primary alkylamine group (R-NH_2) are known to solubilize AgI,[27] we used n-butylamine to prepare the precursor solution. Solution-processed $AgBi_2I_7$ film was fabricated by spin-coating the precursor solution of AgI and BiI_3 (with the molar ratio of 1:2) and subsequently annealing in a nitrogen atmosphere at 150 °C for 30 minutes.

X-ray diffraction (XRD; Figure 1 a) reveals that the crystal structure of $AgBi_2I_7$ is consistent with experimental and calculated XRD results. The $AgBi_2I_7$ film is highly moisture- and air-stable, showing neither structural changes nor phase separation after exposure to ambient conditions for 10 days (Supporting Information, Figure S1). Fitting the experimental data to reference and calculated XRD patterns indicates an $AgBi_2I_7$ film with cubic structure (space group *Fd3m*) with the lattice parameters of $a = b = c = 12.223$ Å, consistent with reported values.[25,26] Furthermore, Rietveld refinement using the $AgBi_2I_7$ crystal structure determined from our XRD results was carried out using the TOPAS-Academic software. The Rietveld analysis confirmed the crystal structure of $AgBi_2I_7$ (Supporting Information, Figure S2).

In previous reports, Ag-Bi-I had been seen to crystallize to other compositions such as Ag_2BiI_5 having a hexagonal structure (space group *R3m*, $a = b = 4.350$ Å, $c = 20.820$ Å).[25,26] We therefore carried out XRD studies on films prepared with a wide range of molar ratios of AgI to BiI_3

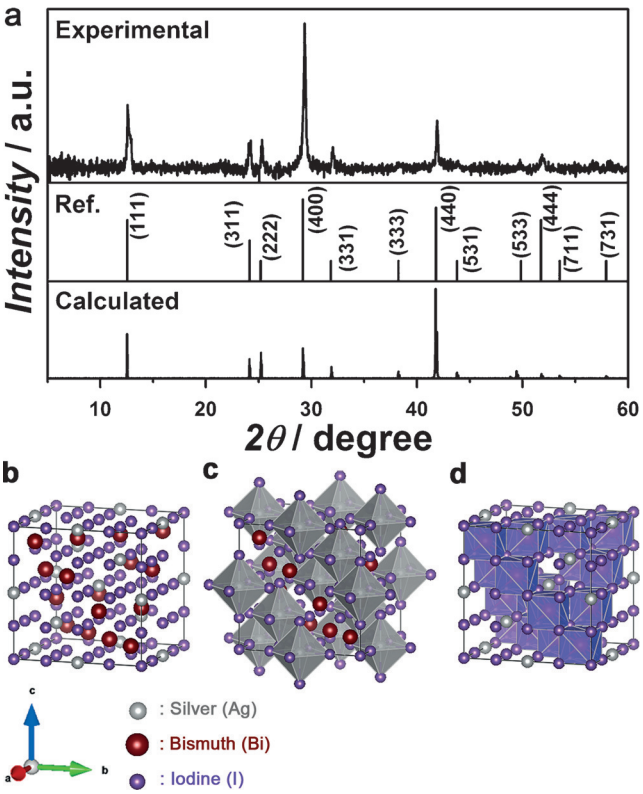

Figure 1. a) Experimental XRD pattern of $AgBi_2I_7$ film. The reference and calculated XRD patterns for $AgBi_2I_7$ were obtained from PDF Card No. 00–034–1372 and computer program VESTA, respectively. b) Representation of the $AgBi_2I_7$ cubic structure (space group *Fd3m*, $a = b = c = 12.223$ Å) with the joint population of a single position by silver, bismuth, and iodide. The unit cell of $AgBi_2I_7$ is expressed with c) six-coordinated silver–iodide octahedron sites and d) eight-coordinated bismuth–iodide hexahedron sites.

(Supporting Information, Figure S3). A single diffraction peak at $2\theta \approx 42°$ is observed in the $AgBi_2I_7$ film used in devices later in this work; but when in these basic studies we used a molar ratio of AgI/BiI_3 that exceeded 1:1, we were able to see the emergence of diffraction peak splitting near $2\theta \approx 42°$: we attribute signals at $2\theta = 41.6°$ and 42.4° to {110} and {108} facets of the Ag_2BiI_5 crystal, respectively.[26] We conclude that, outside the desired process window that produces $AgBi_2I_7$, the ratio of 2:1 yields Ag_2BiI_5 hexagonal-phase crystals. The intended $AgBi_2I_7$ with its cubic structure is controlled by precursor amounts the solution process.

The crystal structure of $AgBi_2I_7$ is illustrated using the computer program VESTA (Figure 1 b). The unit cell of $AgBi_2I_7$ with the cubic structure is densely and symmetrically composed of the joint population of a single position by silver, bismuth, and iodide. Each silver and bismuth metal ion in the $AgBi_2I_7$ unit cell displays a coordination polyhedron of iodides in the form of a silver cation six-coordinated with the octahedral iodide groups and a bismuth cation eight-coordinated with the hexahedral iodide groups (Figures 1 c,d). Furthermore, bismuth iodide hexahedra are connected with silver iodide octahedra via corner-sharing, and thus metal vacancies are not observed in the $AgBi_2I_7$ crystal structure (see the Crystallographic Information File (CIF) in the Supporting Information).

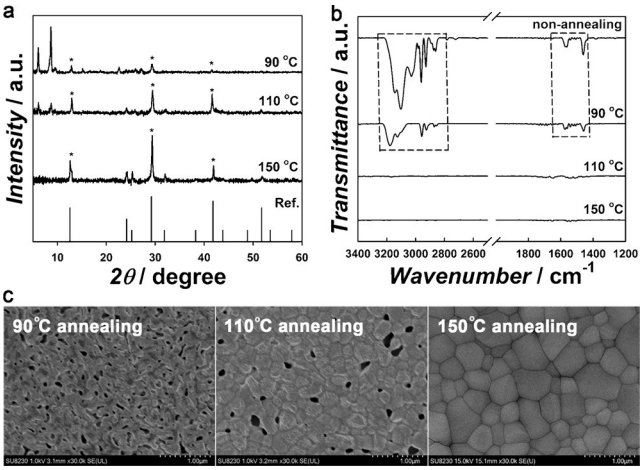

Figure 2. a) XRD patterns, b) FTIR spectra, and c) top-view SEM images of solution-processed Ag-Bi-I thin-films as a function of annealing temperature. The asterisks in (a) indicate the main crystal signals from $AgBi_2I_7$.

The crystallization of $AgBi_2I_7$ is sensitive to annealing temperature. Figure 2a shows a series of such XRD patterns for solution-processed Ag-Bi-I thin-films as a function of annealing temperature for an annealing time of 30 minutes under an nitrogen atmosphere. We confirmed that the spin-cast precursor produces crystallization when heated above 90 °C, forming the cubic-phase indicated by the $AgBi_2I_7$ {111}, {400}, and {440} diffraction peaks at 13, 29, and 42°, respectively. Additionally, this film shows the diffraction peaks at small-angle regions ($2\theta < 10°$), indicating that, at this stage, the film retained the undesired intermediates of bismuth iodide and silver iodide complexes,[22] that is, this had not yet been completely converted to $AgBi_2I_7$.

As the annealing temperature increases above 110 °C, the intensities of the small-angle diffraction signals decrease; and for 150 °C, only the cubic-phase diffractions can be seen, indicating full crystallization of $AgBi_2I_7$.[25,26]

The process of $AgBi_2I_7$ crystallization was investigated further using Fourier transform infrared (FTIR) spectroscopy (Figure 2b). Since n-butylamine was used as the solvent for film preparation, we followed signals associated with this solvent in studies vs. annealing temperature. The FTIR spectrum of as-prepared film (that is, non-annealing) shows strong transmittance peaks for N–H stretching (3200–3600 cm^{-1}), C–H stretching (2850–2980 cm^{-1}), and a weaker peak for N–H bending (1450–1650 cm^{-1}).[28] Although the as-prepared film was thermally annealed at a temperature of 90 °C, a temperature above the boiling point of n-butylamine (77–79 °C), the FTIR spectrum nevertheless retained transmittance peaks that indicated remnant n-butylamine, presumably weakly bound to the BiI_3 and AgI precursors in the form of metal halide–amine complexes.[24,29] These FTIR signals disappeared completely as the annealing temperature increased to 150 °C. When we take these results together with XRD findings, we propose that the Ag-Bi-I precursor film completes its crystallization to cubic-phase $AgBi_2I_7$ at 150 °C via the removal of n-butylamine previously bound to the bismuth iodide and silver iodide complexes.

The surface morphologies of crystallized films annealed at each annealing temperature were characterized using scanning electron microscopy (SEM; Figure 2c). The film annealed at 90 °C does not show the crystallized surface morphologies, a finding that agrees well with the XRD and FTIR observations. As the annealing temperature increases above 110 °C, Ag-Bi-I films yield small grains; and when the temperature was increased to 150 °C, the film became dense and uniform and exhibited grains having sizes 200–800 nm. Neither pinhole nor vacancies are seen in films prepared at 150 °C.

The optical absorption spectra (Figure 3a) of Ag-Bi-I thin films were obtained via UV/Vis spectroscopy. The as-prepared films, yellow to the eye, exhibit a sharp feature at 474 nm, previously reported and associated with isolated bismuth iodide octahedral complexes.[30] The absorption spectra extend into the near IR following annealing at increased temperature: the 150 °C annealed films show substantial absorption over the range 350–750 nm (Supporting Information, Figure S4). We obtained an E_g of 1.87 eV for $AgBi_2I_7$ assuming a direct band gap (Figure 3b). If indirect absorption was instead considered, a value of $E_g \approx 1.66$ eV would be obtained (Supporting Information, Figure S5).

Ultraviolet photoelectron spectroscopy (UPS) was used to determine the Fermi energy (E_f) and the valence band energy (E_v) level of the $AgBi_2I_7$ films (Figure 3c). The E_f was found to be 5.05 eV, determined using the cutoff energy (E_{cutoff}) presented in Figure 3c from the equation $E_f = 21.22$ eV (He I) $- E_{cutoff}$. The linear extrapolation in low binding-energy region indicates the value of ($E_v - E_f$), leading

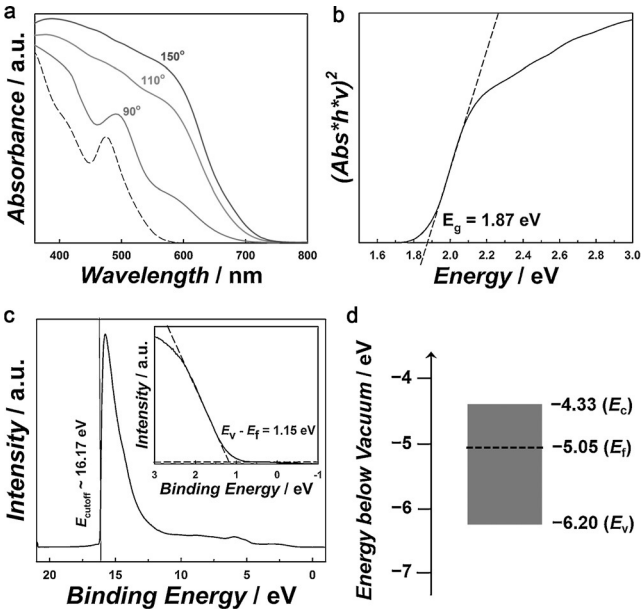

Figure 3. a) UV/Vis spectra of Ag-Bi-I thin-films as a function of annealing temperature. b) Tauc plot of $AgBi_2I_7$ from the UV/Vis spectroscopy to determine E_g under the assumption of a direct band gap. c) UPS spectrum in high binding-energy region of $AgBi_2I_7$ film annealed at 150 °C to determine the E_{cutoff} level. Inset: linear extrapolation in the low-binding-energy region for the value of ($E_v - E_f$). d) Energy band diagram of $AgBi_2I_7$ film calculated from the Tauc plot and UPS results.

to an E_v of 6.2 eV. The conduction band energy (E_c) is then estimated from ($E_v + E_g$), and the band diagram shown as a result in Figure 3d. This analysis suggests substantially intrinsic films.

We fabricated photovoltaic devices using $AgBi_2I_7$ films with high crystallinity and good surface morphologies. Figure 4a shows the cross-sectional SEM image of our solar cell

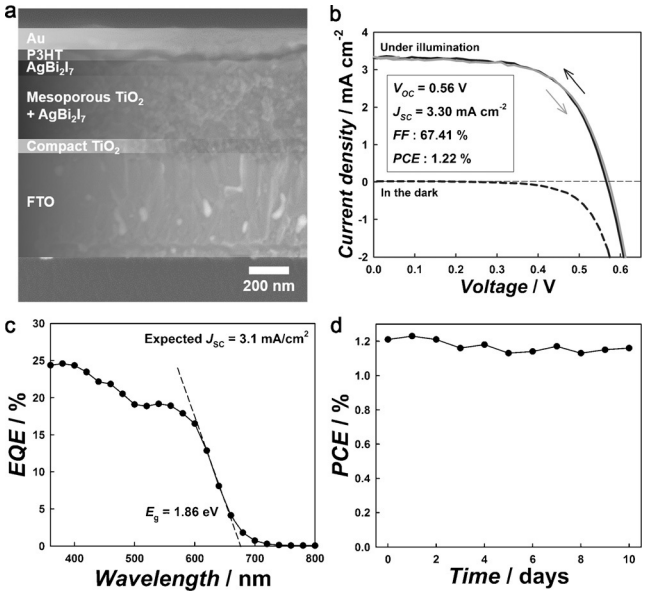

Figure 4. a) Cross-sectional SEM image, b) current-density–voltage (*J-V*) curves in the dark and illumination under 100 mW cm^{-2} AM 1.5 G (area 0.049 cm^2) and device performance values, c) EQE spectrum, and d) device stability (our best solar cell device, stored under ambient conditions).

device prepared with the structure of glass/fluorine-doped tin oxide (FTO) electrode/compact and mesoporous TiO_2/$AgBi_2I_7$/poly(3-hexylthiophene) (P3HT)/gold electrode. Mesoporous TiO_2 and P3HT layers were used as electron transporting and hole transporting materials (ETM and HTM) for our device, respectively.

Figure 4b shows the current-density–voltage (*J-V*) characteristic of an $AgBi_2I_7$ solar cell device measured in the dark and alternatively under illumination using 100 mW cm^{-2} AM 1.5 G. A current density (J_{SC}) of 3.30 mA cm^{-2}, open circuit voltage (V_{OC}) of 0.56 V, fill factor (FF) of 67.41 %, and PCE of 1.22 % were obtained from the best solar cells. The histograms of photovoltaic performance for our 24 solar cell devices are presented in the Supporting Information, Figure S6. Consistent with the optical absorption of $AgBi_2I_7$ film, appreciable external quantum efficiency (EQE) emerged at about 740 nm and increased to 25 %. Furthermore, the E_g (1.86 eV) derived from EQE spectrum agrees with the value (1.87 eV) determined from the Tauc plot. The value obtained from integrating the EQE, $J_{SC} = 3.10$ mA cm^{-2}, agrees well with directly measured J_{SC} (Figure 4c).

To study the origins of the photovoltaic effect in these $AgBi_2I_7$ devices, we fabricated control devices with only mesoporous TiO_2 and P3HT junction (that is, no $AgBi_2I_7$ layer in between). Even though it has been reported that *p*-type P3HT polymer can produce a rectifying junction with n-type TiO_2,[31] our control devices herein showed a PCE below 0.1 % (Supporting Information, Figure S7). The P3HT film on glass substrate has an absorption spectrum ranging from 660 nm to 510 nm (Supporting Information, Figure S8), that is, the EQE features in the $AgBi_2I_7$ were clearly distinct from those of the semiconducting polymer.

We also investigated the device stability of the $AgBi_2I_7$ solar cells. The PCE value of our best device remains above 1.13 % for over 10 days of alternating device storage and testing under ambient conditions (Figure 4d). This is consistent with the high degree of air stability of the underlying active layer (evidenced in the Supporting Information, Figure S1). Moreover, *J-V* curves of $AgBi_2I_7$ solar cells before and after exposure to illumination for 1 h using 100 mW cm^{-2} AM 1.5 G confirm the lack of performance degradation under continuous operation (Supporting Information, Figure S9).

In summary, solution-processed $AgBi_2I_7$ films were prepared using a single-step spin-coating procedure followed by a mild thermal annealing. The device was air-stable and avoided the use of lead and tin. Structural characterization revealed that $AgBi_2I_7$ is crystallized in the cubic-phase with dense surface morphologies via control over the precursor ratio. The $AgBi_2I_7$ film absorption spectrum absorbs light across the range 350 to 750 nm. Further increases in current density represent the largest opportunity to gain performance in this system (advance from ca. 3 mA cm^{-2} to the 25 mA cm^{-2} possible for this band gap): we expect that further advances will be made through the use of mesostructured electrodes (that is, bulk heterojunctions) as well as via deeper studies of transport and trapping in the active medium.

Acknowledgements

This publication is based in part on work supported by Award KUS-11-009-21, made by King Abdullah University of Science and Technology (KAUST), by the Ontario Research Fund—Research Excellence Program, and by the Natural Sciences and Engineering Research Council of Canada (NSERC). The authors thank R. Wolowiec, D. Kopilovic, and E. Palmiano for their technical help over the course of this research. The authors thank Yiying Li (Prof. Zhenghong Lu group, Department of Materials Science and Engineering, University of Toronto) and Dr. Srebri Petrov (Department of Chemistry, University of Toronto) for assistance in UPS measurement and Rietveld refinement analysis.

Keywords: $AgBi_2I_7$ · iodobismuthates · non-toxic photovoltaics · solution processing · thin films

How to cite: *Angew. Chem. Int. Ed.* **2016**, *55*, 9586–9590
Angew. Chem. **2016**, *128*, 9738–9742

[1] U. Bach, D. Lupo, P. Comte, J. E. Moser, F. Weissörtel, J. Salbeck, H. Spreitzer, M. Grätzel, *Nature* **1998**, *395*, 583.
[2] S. A. McDonald, G. Konstantatos, S. Zhang, P. W. Cyr, E. J. D. Klem, L. Levina, E. H. Sargent, *Nat. Mater.* **2005**, *4*, 138.
[3] A. Kojima, K. Teshima, Y. Shirai, T. Miyasaka, *J. Am. Chem. Soc.* **2009**, *131*, 6050.

[4] M. M. Lee, J. Teuscher, T. Miyasaka, T. N. Murakami, H. J. Snaith, *Science* **2012**, *338*, 643.
[5] J. Burschka, N. Pellet, S.-J. Moon, R. Humphry-Baker, P. Gao, M. K. Nazeeruddin, M. Grätzel, *Nature* **2013**, *499*, 316.
[6] W. S. Yang, J. H. Noh, N. J. Jeon, Y. C. Kim, S. Ryu, J. Seo, S. I. Seok, *Science* **2015**, *348*, 1234.
[7] "NREL Efficiency Chart Rev. 03-09-2016," http://www.nrel.gov/ncpv/images/efficiency_chart.jpg, **2016**.
[8] N. K. Noel, S. D. Stranks, A. Abate, C. Wehrenfennig, S. Guarnera, A.-A. Haghighirad, A. Sadhanala, G. E. Eperon, S. K. Pathak, M. B. Johnston, A. Petrozza, L. M. Herz, H. J. Snaith, *Energy Environ. Sci.* **2014**, *7*, 3061.
[9] F. Hao, C. C. Stoumpos, D. H. Cao, R. P. H. Chang, M. G. Kanatzidis, *Nat. Photonics* **2014**, *8*, 489.
[10] A. Babayigit, A. Ethirajan, M. Muller, B. Conings, *Nat. Nanotechnol.* **2016**, *11*, 247.
[11] D. B. Mitzi, *Inorg. Chem.* **2000**, *39*, 6107.
[12] D. B. Mitzi, P. Brock, *Inorg. Chem.* **2001**, *40*, 2096.
[13] B.-W. Park, B. Philippe, X. Zhang, H. Rensmo, G. Boschloo, E. M. J. Johansson, *Adv. Mater.* **2015**, *27*, 6806.
[14] R. L. Z. Hoye, R. E. Brandt, A. Osherov, V. Stevanović, S. D. Stranks, M. W. B. Wilson, H. Kim, A. J. Akey, J. D. Perkins, R. C. Kurchin, J. R. Poindexter, E. N. Wang, M. G. Bawendi, V. Bulović, T. Buonassisi, *Chem. Eur. J.* **2016**, *22*, 2605.
[15] M. Lyu, J.-H. Yun, M. Cai, Y. Jiao, P. V. Bernhardt, M. Zhang, Q. Wang, A. Du, H. Wang, G. Liu, L. Wang, *Nano Res.* **2016**, *9*, 692.
[16] A. J. Lehner, H. Wang, D. H. Fabini, C. D. Liman, C.-A. Hébert, E. E. Perry, M. Wang, G. C. Bazan, M. L. Chabinyc, R. Seshadri, *Appl. Phys. Lett.* **2015**, *107*, 131109.
[17] R. E. Brandt, V. Stevanović, D. S. Ginley, T. Buonassisi, *MRS Commun.* **2015**, *5*, 265.
[18] A. H. Slavney, T. He, A. M. Lindenberg, H. I. Karunadasa, *J. Am. Chem. Soc.* **2016**, *138*, 2138.
[19] E. T. McClure, M. R. Ball, W. Windl, P. M. Woodward, *Chem. Mater.* **2016**, *28*, 1348.
[20] C. Feldmann, *Inorg. Chem.* **2001**, *40*, 818.
[21] W.-X. Chai, L.-M. Wu, J.-Q. Li, L. Chen, *Inorg. Chem.* **2007**, *46*, 1042.
[22] W.-X. Chai, L.-M. Wu, J.-Q. Li, L. Chen, *Inorg. Chem.* **2007**, *46*, 8698.
[23] N. Louvain, N. Mercier, F. Boucher, *Inorg. Chem.* **2009**, *48*, 879.
[24] N. Mercier, N. Louvain, W. Bi, *CrystEngComm* **2009**, *11*, 720.
[25] P. H. Fourcroy, M. Palazzi, J. Rivet, J. Flahaut, R. Céolin, *Mater. Res. Bull.* **1979**, *14*, 325.
[26] L. F. Mashadieva, Z. S. Aliev, A. V. Shevelkov, M. B. Babanly, *J. Alloys Compd.* **2012**, *524*, 38.
[27] L. E. Topol, H. Mandel, US Patent 3 719 611, **1973**.
[28] G. Konstantatos, I. Howard, A. Fischer, S. Hoogland, J. Clifford, E. Klem, L. Levina, E. H. Sargent, *Nature* **2006**, *442*, 180.
[29] E. M. Marlett, US Patent 5 045 244, **1991**.
[30] X.-H. Zhu, N. Mercier, P. Frère, P. Blanchard, J. Roncali, M. Allain, C. Pasquier, A. Riou, *Inorg. Chem.* **2003**, *42*, 5330.
[31] C. Y. Kuo, W. C. Tang, C. Gau, T. F. Guo, D. Z. Jeng, *Appl. Phys. Lett.* **2008**, *93*, 033307.

Received: April 13, 2016
Revised: May 31, 2016
Published online: June 29, 2016

